




Frequency-tunable transient Cherenkov radiation from an inhomogeneous mediumAnton Pakhomov  and Rostislav Arkhipov *Faculty of Physics, St. Petersburg State University, Universitetskaya Embankment 7/9, St. Petersburg 199034, Russia* (Received 10 May 2021; revised 5 August 2021; accepted 26 August 2021; published 8 September 2021)

We propose a scheme to generate coherent radiation with a tunable frequency spectrum based on the excitation of an inhomogeneous thin layer of a resonant medium by an ultrashort pulse. The Cherenkov-type radiation emitted in a transient stage, i.e., while the excitation wavefront is still propagating over the medium, is shown to contain additional frequency components, which are determined by the spatial frequency components of the medium's density distribution and the excitation geometry. We demonstrate that the spectral content of this transient radiation can be adjusted in wide limits by controlling the spatial density distribution of the resonant medium and the shape of the excitation wavefront. Our theoretical results pave the way towards simple and compact swept-frequency or frequency-tunable optical oscillators as well as sources of the frequency-modulated optical radiation.

DOI: [10.1103/PhysRevA.104.033509](https://doi.org/10.1103/PhysRevA.104.033509)**I. INTRODUCTION**

Cherenkov radiation is the well-known phenomenon arising when a charged particle moves through a dielectric medium with a speed greater than the speed of light in this medium [1–4]. Cherenkov radiation emanates within a cone with the cone angle determined by the ratio of the particle's speed and the speed of light in the medium. Cherenkov radiation has found multiple applications so far in detection and identification of high-energy charged particles in biomedical imaging, astrophysics, and particle physics [2–10]. Besides the charged particles, Cherenkov radiation was also found to be generated by many propagating optical waves, such as surface polaritons in metal-dielectric structures [11], a superluminal spot of nonlinear polarization [12], and optical solitons [13,14]. Finally, there are some nonphysical objects which can propagate at superluminal velocities and can act as sources of coherent electromagnetic radiation, including Cherenkov radiation [15–18]. Among them are a spot of light on a remote screen from a source rapidly rotating with a constant angular velocity [15] and a spot of light arising when a plane wavefront of an ultrashort pulse is incident on a flat surface at an angle β [15]. In the latter case, the cross-section point of the wavefront and the medium moves along the medium with a superluminal velocity $V = c/\sin \beta > c$. It should be noted that such medium excitation at superluminal velocities does not violate the relativity theory. Indeed, the relativity theory only prohibits the energy transfer with superluminal velocities. At the same time the superluminal motion of the intersection point and thus the superluminal excitation of the medium's oscillators is not accompanied by such energy transfer. The superluminal energy transfer would imply that the wave from a source of the excitation pulse has reached some point of the medium faster than the light in vacuum would do, which in fact does not occur, since neither the excitation pulse nor the secondary radiation from

the medium's oscillators propagate with velocities faster than the vacuum speed of light.

Cherenkov radiation also has been investigated in different spatially inhomogeneous media. The motion of a charged particle above a periodic grating was found to give rise to the Cherenkov-type radiation phenomenon known as the Smith-Purcell effect [19,20]. In recent years Cherenkov radiation has been actively studied in photonic crystals and metamaterials [21–25] and a number of unusual features of the Cherenkov radiation were discovered in such media. In particular, those include the absence of a velocity threshold for the observation of the Cherenkov radiation [26–31], the possibility of a backward-pointing radiation cone [32,33], and polarization manipulation [34].

Among features, the spectral properties of Cherenkov radiation attract a great deal of interest. The classical Cherenkov radiation of a moving charge in a dielectric medium exhibits a broad and rather unstructured frequency spectrum [3]. However, multiple studies on Cherenkov radiation in spatially inhomogeneous periodic dielectric media, specifically in photonic crystals, showed the possibility of obtaining coherent Cherenkov radiation at a certain frequency with a very narrow frequency band [21,22]. Such frequency-tunable Cherenkov radiation was found when a charged particle moves near a periodic grating structure which possesses photonic bound states in the continuum (BICs) and quasi-BICs [35]. The highly coherent Cherenkov radiation was also generated by a collectively interacting beam of free electrons rather than a single point charge while traveling through a photonic crystal [36]. In all these cases the operating frequency could be varied over a wide range by adjusting the period of the photonic crystal, which does not seem very convenient for applications, where the frequency needs to be largely tuned or the whole range of frequencies has to be excited.

Another alternative approach to obtaining Cherenkov radiation at a specific desired frequency was proposed in Ref. [37],

where the transient Cherenkov radiation from a string of oscillators with periodic density when excited by a superluminal spot of light was considered. It was found that, when an ultrashort pulse excites the string at a superluminal velocity [18], the spectrum of the Cherenkov radiation contains, besides the resonant frequency of oscillators, another frequency, proportional to the spatial frequency of the oscillators' density distribution. In subsequent work [38] the transient Cherenkov radiation from a circular string of oscillators excited by a superluminal spot of light moving along the circle was studied in detail. The possibility of Cherenkov radiation control in a one-dimensional string of oscillators excited by ultrashort pulse trains at a superluminal velocity was investigated in [39].

However, this phenomenon of Cherenkov radiation described above was only considered in a one-dimensional string of oscillators with harmonic spatial density and a plane excitation wavefront. As a result, only one additional frequency of the transient radiation was obtained. At the same time, additional degrees of freedom for the control of the medium radiation can be provided by more complex spatial density variations in a two-dimensional array of oscillators as well as by curved excitation wavefronts, as it was outlined in [40].

In this paper, we study Cherenkov radiation from a thin layer of a resonant medium with spatially inhomogeneous density upon excitation by an ultrashort pulse with an arbitrary shape of the wavefront. We remark that in our case Cherenkov radiation occurs due to the collective coherent phenomenon of free-induction decay arising when a resonant medium is excited by an ultrashort pulse with duration shorter than the medium polarization relaxation time T_2 [41]. We demonstrate that the response of a medium contains, besides the resonant frequency of medium oscillators, also extra frequency components due to the spatially varying medium density upon the excitation. We consider different geometries of the medium as well as different types of excitation sources and show that these additional frequencies can be largely and easily tuned in wide limits and can also fill the whole frequency range, whose borders depend on the problem parameters. Our findings therefore provide a convenient and technologically feasible concept for implementing a frequency-tunable source of coherent Cherenkov radiation with large flexibility in the frequency control.

This paper is organized as follows. In Sec. II we present the system under consideration and provide the underlying physical background. In Secs. III and IV we consider several possible excitation geometries for the constant excitation velocity and the varying excitation velocity, respectively, and analyze the radiation spectrum for each case. A summary and concluding remarks are provided in Sec. V.

II. MODEL STATEMENT

We assume that the medium oscillators are described by the standard Lorentz model [41]

$$\ddot{\vec{P}} + 2\gamma\dot{\vec{P}} + \omega_0^2\vec{P} = g_0\vec{E}(t), \quad (1)$$

with the resonant frequency ω_0 , the damping rate $\gamma = 1/T_2$, and the medium coupling strength g_0 to a pump field $\vec{E}(t)$. As the oscillators one can take, for instance, two-level atoms [41],

semiconductor quantum dots [42–44], or metallic nanoantennas [45–47].

In Ref. [37] it was found that the Cherenkov radiation from a linear inhomogeneous string of Lorentz oscillators, when excited by an ultrashort pulse, at the transient stage, i.e., while the excitation pulse is propagating over the string, contains a new frequency component given as

$$\Omega = 2\pi \frac{V/\Lambda}{|V \cos \alpha/c - 1|}. \quad (2)$$

Here α is the observation angle, Λ is the period of the density modulation, and V is the superluminal velocity at which the intersection point of the wavefront of the exciting pulse and the string of oscillators moves along the string. Since this velocity is always higher than the speed of light $V \geq c$, the frequency (2) goes to infinity, when

$$\cos \alpha = \frac{c}{V}. \quad (3)$$

The condition (3) actually implies that the observation angle equals the angle between the string and the excitation wavefront; hence all oscillators radiate in phase in this particular direction and no additional modulation of the emitted signal appears.

After an ultrashort pulse-driven excitation the medium polarization oscillates within the time $T_2 = \gamma^{-1}$ [41]. As a result, a medium radiates Cherenkov-type radiation via the collective spontaneous emission related to the free-induction decay [48,49]. Such a superradiantlike mechanism can be attractive for the generation of broadband ultrashort pulses in UV and THz frequency ranges (for a review see [50] and references therein). As it was shown in [51,52], the response of a linear oscillator (1) subject to a sudden excitation can be described as

$$E(t) = E_0 e^{-\gamma(t-t_0)} \cos \omega_0(t-t_0), \quad t \geq t_0, \quad (4)$$

where t_0 is the time point of the excitation. The sudden excitation means that the duration of the driving ultrashort pulse is much shorter than the period of the resonant oscillations $2\pi/\omega_0$. It is worth noting that the oscillator's response in the form (4) is only valid after the excitation pulse has passed the oscillator. At the same time during the action of the excitation pulse, additional field bursts will be emitted by the oscillator preceding the response (4). In the following we will not take these bursts into account and use Eq. (4). On the one hand, this would greatly simplify the derivations and allows us to obtain some analytical expressions. On the other hand, as we will show below, this simplification does not influence the validity of our results.

Let us suppose now that we have a two-dimensional array of Lorentz oscillators (1) distributed with a spatial density $\rho(x, y)$. The thickness of such an array is assumed to be much smaller than the wavelength of the medium resonant oscillations. In this case one can reliably neglect the reverse action of the medium radiation on the excitation pulse and therefore suppose that all oscillators in the array are driven by the same pump pulse. The total response of the array is then given as the sum of the responses of each single oscillator (4) with certain time delays between them appearing both due to the excitation delay as the pump pulse propagates over the

array with a finite velocity and due to the varying distance from an arbitrary point of the medium to the observer. Using Eq. (4), the field emitted from the array is given by the integral [37]

$$E(t) = E_0 \int_0^{L_x} \int_0^{L_y} e^{-\gamma(t-\tau(x,y))} \cos \omega_0(t - \tau(x,y)) \times \Theta(t - \tau(x,y)) D(\vec{n}_E - \vec{n}_O) \rho(x,y) dx dy, \quad (5)$$

with a constant E_0 corresponding to a field from a single oscillator and the Heaviside step function Θ . The factor $D(\vec{n}_E - \vec{n}_O)$ describes the angular radiation pattern of a single dipole emitter, where \vec{n}_E is the unit vector directed along the polarization direction of the excitation pulse and \vec{n}_O is the unit vector pointing in the direction of the observer, and is given as [53]

$$D(\vec{n}_E - \vec{n}_O) = \sin(\arccos \vec{n}_E \vec{n}_O). \quad (6)$$

Equation (5) contains several functions to be specified for a particular system geometry. The delay function $\tau(x,y)$ describes the time point when the excitation pulse reaches the point of the medium with the coordinates (x,y) as well as the respective delay in the emission propagation to the observer. Here $\rho(x,y)$ is the spatial density of the oscillators' distribution. We will mainly use the periodic density in both coordinates

$$\rho(x,y) = \rho_0(1 + A_x \cos \Lambda_x x)(1 + A_y \cos \Lambda_y y), \quad (7)$$

with the spatial frequencies Λ_x and Λ_y and the amplitudes of the density variations $A_x, A_y \leq 1$. Such spatial density variations can be made artificially using modern techniques of micro- and nanopatterning of the nanoantenna or quantum-dot arrays or, for instance, by exciting an intense acoustic wave in an optically thin dielectric plate.

III. CONSTANT EXCITATION VELOCITY

We start with the case of the constant excitation velocity. Therefore, we assume that our two-dimensional array of oscillators (7) is excited by a few-cycle pulse possessing a plane wavefront. We take the normal to the excitation wavefront to form the angle θ with the plane of the array and the angle φ with the x axis in the plane of the array. Further, the observer is supposed to be located at a distant point so that the observation direction forms an angle α with the array's plane and its in-plane projection forms the angle β with the x axis in the plane of the array (see Fig. 1). In this case the delay function $\tau(x,y)$ is given as

$$\tau(x,y) = \frac{R_0}{c} + \frac{x \cos \varphi + y \sin \varphi}{c/\cos \theta} - \cos \alpha \frac{x \cos \beta + y \sin \beta}{c}, \quad (8)$$

where R_0 is the distance between the origin of coordinates and the observation point.

We can also specify now the extra factor $D(\vec{n}_E - \vec{n}_O) = D(\alpha, \beta, \varphi)$ in the integral (5), which accounts for the linear polarization of the exciting pulse. This factor describes the angular shape of the dipole emission of the medium oscillators

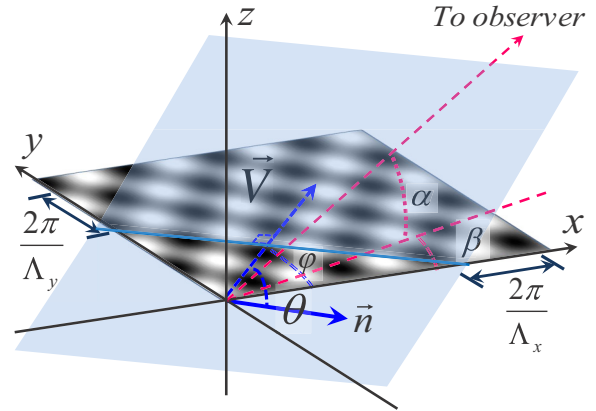


FIG. 1. An optically thin layer of a resonant medium with the spatially inhomogeneous density (the spatial frequencies of the density distribution are Λ_x and Λ_y over the x and y axes, respectively) is irradiated by a linearly polarized ultrashort pulse with the plane wavefront (shaded blue) so that the intersection line of the wavefront and the medium (dashed blue line) propagates with the superluminal velocity $V = c/\cos \theta > c$ over the medium. The medium radiation is detected at a distant point and the observation direction is determined by the angles α and β . The angle between the normal to the wavefront and the plane of the array is θ and the angle between the velocity vector \vec{V} and the x axis in the plane of the array is φ

and in the case of a TE-polarized excitation pulse according to Eq. (6) is given as

$$D(\alpha, \beta, \varphi) = \sin\{\arccos[\cos \alpha \sin(\varphi - \beta)]\}, \quad (9)$$

i.e., constant across the whole layer. Besides that, it is worth noting that the field of a single oscillator E_0 in Eq. (5) depends on the distance R_0 as [53]

$$E_0 \sim \frac{1}{R_0}.$$

The integral (5) with the periodic spatial density (7) and the delay function (8) can be calculated analytically. The corresponding derivation is provided in the Appendix. It is convenient to introduce the values

$$\begin{aligned} t' &= t - \frac{R_0}{c}, \\ q_x &= \omega_0 \frac{\cos \theta \cos \varphi - \cos \alpha \cos \beta}{c}, \\ q_y &= \omega_0 \frac{\cos \theta \sin \varphi - \cos \alpha \sin \beta}{c} \end{aligned} \quad (10)$$

so that one can rewrite, in Eq. (5),

$$\omega_0(t - \tau(x,y)) = \omega_0 t' - q_x x - q_y y.$$

Then, as shown in the Appendix, the spectrum of the radiation at the transient stage, i.e., while the excitation pulse is propagating across the medium, contains two additional frequencies, namely,

$$\Omega_1 = \frac{\Lambda_x \omega_0}{q_x} = \frac{\Lambda_x c}{\cos \theta \cos \varphi - \cos \alpha \cos \beta} \quad (11)$$

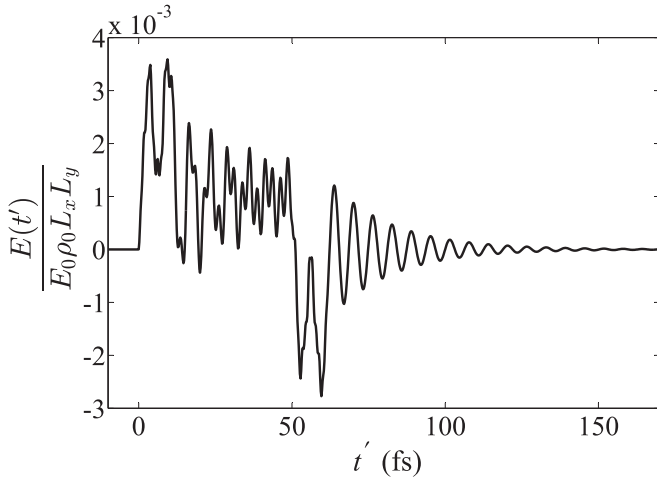


FIG. 2. Radiation from a thin layer of a spatially inhomogeneous medium shown in Fig. 1 for the parameter values $L_x = 60 \mu\text{m}$, $L_y = 50 \mu\text{m}$, $\omega_0 = 10^{15} \text{s}^{-1}$, $\gamma = 5 \times 10^{13} \text{s}^{-1}$, $\alpha = 5\pi/12$, $\beta = \pi/4$, $\theta = \pi/3$, $\varphi = \pi/6$, $A_x = A_y = 1$, $2\pi/\Lambda_x = 3 \mu\text{m}$, and $2\pi/\Lambda_y = 5 \mu\text{m}$. With these parameters Eqs. (11) and (12) yield $\Omega_1 = 2.51 \times 10^{15} \text{s}^{-1}$ and $\Omega_2 = 5.63 \times 10^{15} \text{s}^{-1}$.

and

$$\Omega_2 = \frac{\Lambda_y \omega_0}{q_y} = \frac{\Lambda_y c}{\cos \theta \sin \varphi - \cos \alpha \sin \beta}. \quad (12)$$

In the one-dimensional case obtained, Eqs. (11) and (12) coincide with Eq. (2), keeping in mind the notation used.

Figure 2 shows an example of the radiated field from a spatially inhomogeneous medium for the parameter values $L_x = 60 \mu\text{m}$, $L_y = 50 \mu\text{m}$, $\omega_0 = 10^{15} \text{s}^{-1}$, $\gamma = 5 \times 10^{13} \text{s}^{-1}$, $\alpha = 5\pi/12$, $\beta = \pi/4$, $\theta = \pi/3$, $\varphi = \pi/6$, $A_x = A_y = 1$, $2\pi/\Lambda_x = 3 \mu\text{m}$, and $2\pi/\Lambda_y = 5 \mu\text{m}$. Using Eqs. (11) and (12), we find, for the frequencies of the transient Cherenkov radiation, $\Omega_1 = 2.51 \times 10^{15} \text{s}^{-1}$ and $\Omega_2 = 5.63 \times 10^{15} \text{s}^{-1}$, so both frequencies are well separated from the medium's resonant frequency ω_0 in the spectrum. The detected field in the considered example would represent the superposition of the harmonic oscillations with three incommensurate frequencies ω_0 , Ω_1 , and Ω_2 in the interval $0 \leq t' \leq q_x L_x + q_y L_y = 61.2 \text{ fs}$, followed by the damped oscillations at the frequency ω_0 . The respective frequency spectrum is plotted in Fig. 3. One can indeed see three well-pronounced peaks at the frequencies ω_0 , Ω_1 , and Ω_2 . The relative strengths of these three peaks are determined by the system parameters, as provided in the Appendix. At the same time the peaks at the frequencies Ω_1 and Ω_2 can be easily made stronger by increasing the dimensions of the medium layers L_x and L_y , which would increase the duration of the time interval $0 \leq t' \leq q_x L_x + q_y L_y$, where the corresponding oscillations occur. Also varying the incidence angles and/or the observation angles, one can easily tune the detected transient frequencies (11) and (12) in rather wide limits.

It is important to note that the frequencies (11) and (12) do not depend on the medium's resonant frequency ω_0 , but are only determined by the parameters of the oscillators' density distribution and the excitation geometry. This fact allows generalizing our main findings to the case of an arbitrary optical

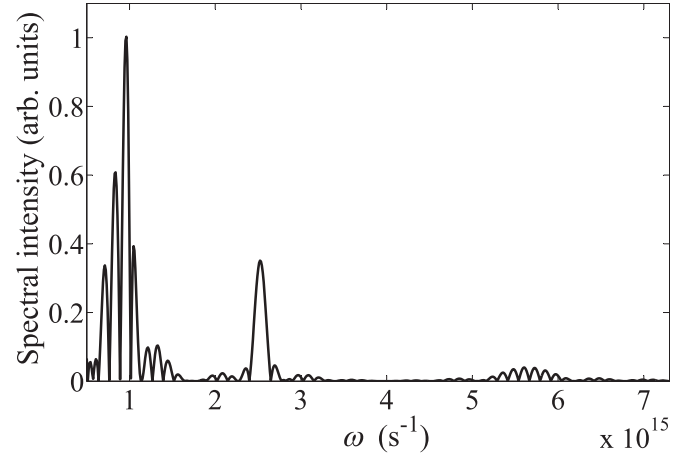


FIG. 3. Spectrum of the radiation from Fig. 2 for $\omega_0 = 10^{15} \text{s}^{-1}$, $\Omega_1 = 2.51 \times 10^{15} \text{s}^{-1}$, and $\Omega_2 = 5.63 \times 10^{15} \text{s}^{-1}$.

medium. Indeed, the response of a single oscillator provided by Eq. (4) was specifically derived for a Lorentz oscillator (1) under the sudden pulsed excitation [51,52]. Otherwise, if one applies a more complex model to describe the optical response of a resonant oscillator, the temporal shape of the oscillator's response would be given by another function instead of Eq. (4). However, an arbitrary function can be expanded into the temporal Fourier series or the Fourier integral, i.e., represented as a superposition of harmonic functions with different frequencies. Since Eq. (5) is linear over the medium's response, this would turn Eq. (5) into the linear superposition of such integrals from harmonic functions. Each of these integrals, as shown in the Appendix, yields, besides the corresponding frequency, also the additional transient frequencies (11) and (12). Since these transient frequencies are independent of ω_0 , they would arise when calculating the integral (5) for each Fourier component in the medium's response. Therefore, the frequencies (11) and (12) would inevitably appear in the spectrum of the detected radiation, regardless of the specific choice of the model of medium's oscillators.

Furthermore, it is also of interest to examine the possible range of the values of the transient frequencies (11) and (12). One can easily see that the lower limits are

$$\begin{aligned} \Omega_1^{\text{lower}} &= \Lambda_x c, \\ \Omega_2^{\text{lower}} &= \Lambda_y c \end{aligned} \quad (13)$$

and can be achieved for the specific angle values when the denominators of Eqs. (11) and (12) become 1. At the same time there are no finite upper limits for Ω_1 and Ω_2 . Indeed, when the denominators of Eqs. (11) and (12) become 0, both transient frequencies become infinite, while for an arbitrary finite frequency exceeding the values (13), one can easily find such angle values that the expressions (11) and (12) provide exactly this required value. Therefore, by varying the excitation and observation angles we can tune the measured transient frequency in wide limits using the same layer of a spatially inhomogeneous medium. Let us suppose, for example, that we can artificially create an inhomogeneous distribution of the resonant oscillators with the spatial period of the order of ten of microns. The respective lower limits

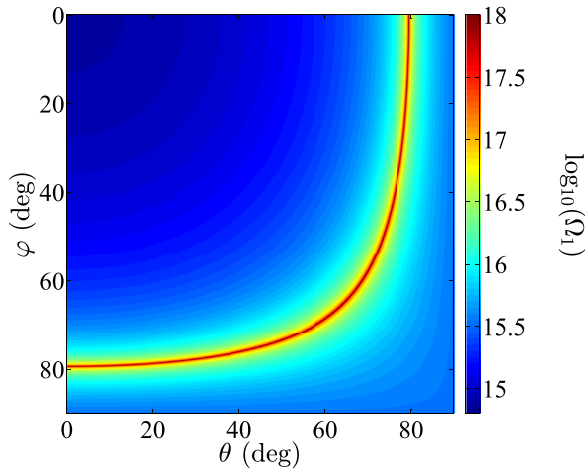


FIG. 4. Diagram showing the dependence of the transient Cherenkov frequency Ω_1 from Eq. (11) vs the angles φ and θ , as defined in Fig. 1. The values of the observation angles are fixed to $\alpha = 5\pi/12$ and $\beta = \pi/4$. Here Ω_1 is assumed to be expressed in s^{-1} and plotted in logarithmic scale. The red curve corresponds to the divergence of the Ω_1 value (for clarity, the color scale is adjusted to the finite top value of $10^{18} s^{-1}$).

of the measured transient frequencies (13) would fall into the mid-IR range; thus the whole visible and ultraviolet ranges can be covered by the described transient Cherenkov radiation through the respective choice of the geometry parameters.

In Figs. 4 and 5 we have plotted the diagrams showing the values of the transient Cherenkov frequencies (11) and (12) vs the angles φ and θ (see Fig. 1). Here we have fixed the values $\alpha = 5\pi/12$ and $\beta = \pi/4$, as in Figs. 2 and 3. The values of Ω_1 and Ω_2 are shown in the logarithmic scale, with Ω_1 and Ω_2 expressed in s^{-1} . One can easily see the curves of the divergence points, where the values of Ω_1 and Ω_2 go to infinity

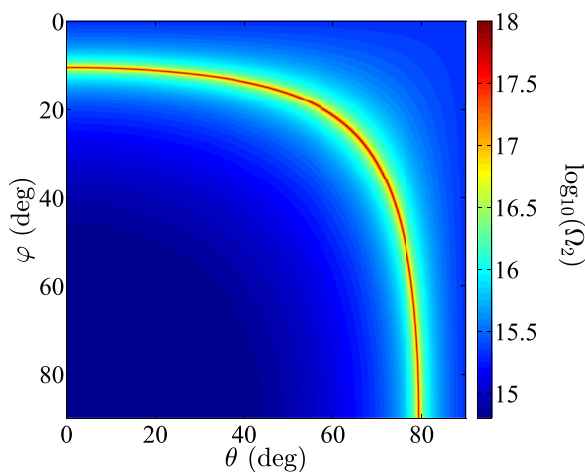


FIG. 5. Diagram showing the dependence of the transient Cherenkov frequency Ω_2 from Eq. (12) vs the angles φ and θ , as defined in Fig. 1. The values of the observation angles are fixed to $\alpha = 5\pi/12$ and $\beta = \pi/4$. Here Ω_2 is assumed to be expressed in s^{-1} and plotted in logarithmic scale. The red curve corresponds to the divergence of the Ω_2 value (for clarity, the color scale is adjusted to the finite top value of $10^{18} s^{-1}$).

(for illustration purposes we restricted the top values in the diagrams). The physical meaning of this case is the absence of the transient Cherenkov radiation, when observed under these specific angles, because all oscillators emit exactly in phase in the corresponding observation directions. Therefore, the spatial distribution of the oscillators does not play any role for such the combinations of the observation and excitation angles.

Equations (11) and (12) correspond to the case when the spatial density distribution (7) represents a harmonic function over each spatial coordinate. One can easily extend these findings to the case of an arbitrary spatial density of the oscillators' distribution $\rho(x, y)$. Indeed, the integral (5) is linear over the factor $\rho(x, y)$. Therefore, if the function $\rho(x, y)$ contains other spatial Fourier components, except for (Λ_x, Λ_y) , the spectrum of the transient radiation would contain, similar to Eqs. (11) and (12), additional respective frequency components. For definiteness, let us assume that the spatial density $\rho(x, y)$ possesses extra spatial Fourier components (κ_x, κ_y) . Then in the frequency spectrum of the transient radiation besides the components (11) and (12), one would measure two other components

$$\Omega = \frac{\kappa_x \omega_0}{q_x}, \frac{\kappa_y \omega_0}{q_y}. \quad (14)$$

In a similar way, if the spatial Fourier spectrum of $\rho(x, y)$ contains the whole range of spatial frequencies, the corresponding frequency spectrum of the transient radiation would contain a similar range.

To illustrate this result, we consider an exemplary spatial modulation of the oscillators' density, similar to Eq. (7), but with nonconstant spatial periods. Namely, for $\rho(x, y)$ we take the expression

$$\rho(x, y) = \rho_0 \left[1 + A_x \cos \Lambda_x \left(1 + \frac{x}{4L_x} \right) x \right] \times \left[1 + A_y \cos \Lambda_y \left(1 + \frac{y}{4L_y} \right) y \right], \quad (15)$$

i.e., the harmoniclike function over each coordinate with slowly varying periods. Specifically, the spatial frequency of the density modulation along the x axis given as

$$\frac{\partial}{\partial x} \Lambda_x \left(1 + \frac{x}{4L_x} \right) x = \Lambda_x \left(1 + \frac{x}{2L_x} \right)$$

increases from Λ_x at $x = 0$ to $1.5\Lambda_x$ at $x = L_x$; the same holds for the y axis. According to the reasoning above, in the spectrum of the detected Cherenkov radiation, we anticipate to obtain the whole continuous range of the transient frequencies (11) and (12), starting at the peaks shown in Fig. 3 and extending up to 1.5 higher upper boundaries. The actual calculation results are plotted in Figs. 6 and 7. From a comparison of the field spectra in Figs. 3 and 7 one can see that the single peaks of the transient radiation indeed get converted into the continuous frequency intervals with the boundaries determined by the range of spatial frequencies of the density modulation. We can therefore tune the frequency of the measured Cherenkov radiation by controlling the medium's density distribution.

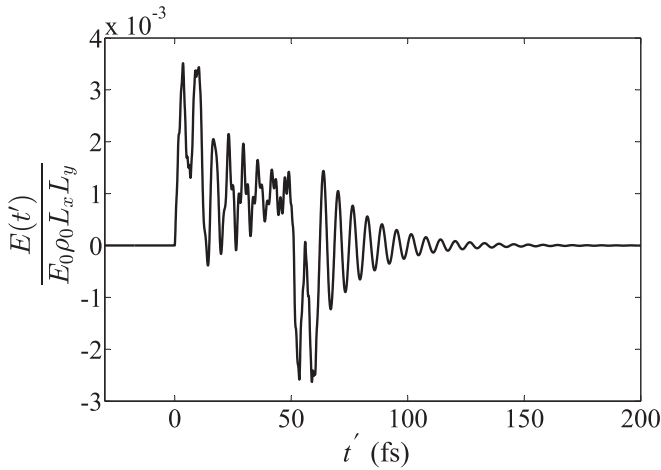


FIG. 6. Radiation from a thin layer of a spatially inhomogeneous medium shown in Fig. 1 under the excitation by a plane wavefront for the same parameter values as in Fig. 2, but for the slowly varying periods of the medium's density modulation from Eq. (15).

IV. VARYING EXCITATION VELOCITY

Controlling the density modulation represents just one of the possible ways to tune the frequency of the transient Cherenkov radiation. Other possibilities based on the control of the excitation velocity seem to be more attractive, since varying the incidence angle of the excitation wavefront can be rather easily achieved in experiments.

Given that, let us now turn to the case of the varying excitation velocity. The simplest way to implement this is to excite the array (7) by a pulse possessing a curved wavefront. We start with the case of a cylindrical wavefront of a linearly polarized excitation ultrashort pulse. The respective layout is schematically depicted in Fig. 8. The axis of the cylindrical wavefront is located at the height H above the medium and its projection on the medium plane crosses the x axis at the point D_x . The angle between the projection of the normal to the cylinder axis on the plane of the array and the x axis is fixed throughout the whole array and equals φ . The cylindrical wave is assumed to be linearly polarized along the cylinder

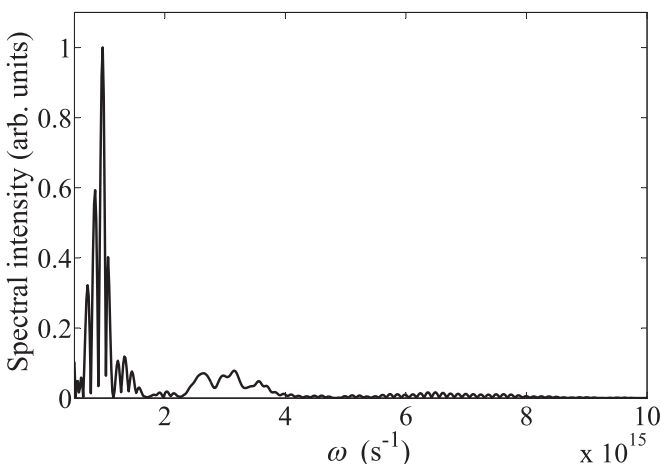


FIG. 7. Spectrum of the radiation from Fig. 6 for $\omega_0 = 10^{15} \text{ s}^{-1}$.

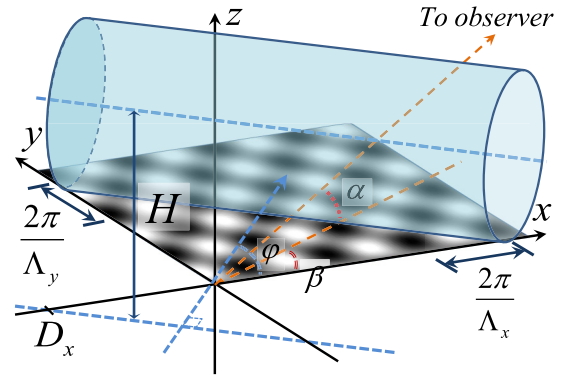


FIG. 8. An optically thin layer of a resonant medium with a spatially inhomogeneous density (the spatial frequencies of the density distribution are Λ_x and Λ_y over the x and y axes, respectively) is irradiated by a linearly polarized ultrashort pulse with a cylindrical wavefront (shaded blue). The cylinder axis of the source of the cylindrical wave is located at the height H above the medium and its projection on the medium's plane is shifted along the x axis for D_x . The normal to the cylinder axis projected on the plane of the array forms the fixed angle φ with the x axis. The medium radiation is detected at a distant point and the observation direction is determined by the angles α and β .

axis. The delay function $\tau(x, y)$ in this case can be expressed as

$$\tau(x, y) = \frac{R_0}{c} + \frac{\sqrt{H^2 + [(x - D_x) \cos \varphi + y \sin \varphi]^2}}{c} - \cos \alpha \frac{x \cos \beta + y \sin \beta}{c}. \quad (16)$$

As compared to the plane wavefront in Fig. 1, we actually get the excitation with the fixed φ angle, but varying angle θ across the medium layer. Since the excitation pulse has a fixed polarization direction, the angular factor $D(\alpha, \beta, \varphi)$ is still given by Eq. (9) and is constant across the whole layer. As the instantaneous value of θ changes, the frequencies (11) and (12) run over the values within a certain interval. The boundaries of this interval can be found from the diagrams in Figs. 4 and 5. Since the frequencies (11) and (12) diverge at certain values of θ , two options are possible depending on whether the point of divergence falls in the range of θ values. If it does, the instantaneous values of the transient frequencies (11) and (12) run over an infinite range during the finite time interval, so the respective spectrum would be “smeared” over the infinite frequency range and would be barely observable. In contrast, if the divergence point does not fall in the range of θ values, one would get a finite interval of instantaneous values of the transient frequencies (11) and (12). In this case we should obtain the corresponding frequency range in the measured spectrum whose boundaries can be easily tuned by the parameters of the excitation geometry.

Figure 9 demonstrates the calculated field from the layer upon excitation by a cylindrical wavefront for the latter case, when the finite range of transient frequencies is expected to appear. Here we have increased the medium's resonant frequency to $\omega_0 = 10^{16} \text{ s}^{-1}$ to make sure that the frequencies of the transient Cherenkov radiation are well separated in the

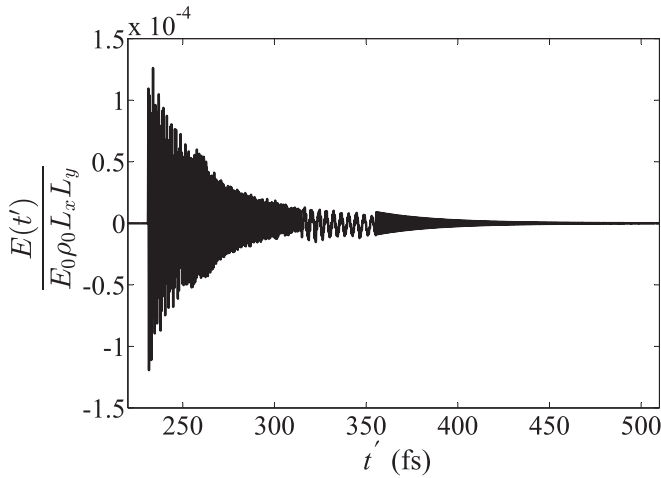


FIG. 9. Radiation from a thin layer of a spatially inhomogeneous medium excited by a cylindrical wavefront as shown in Fig. 8 for the parameter values $L_x = 60 \mu\text{m}$, $L_y = 50 \mu\text{m}$, $\omega_0 = 10^{16} \text{s}^{-1}$, $\gamma = 5 \times 10^{13} \text{s}^{-1}$, $\alpha = 5\pi/12$, $\beta = \pi/4$, $\varphi = \pi/6$, $A_x = A_y = 1$, $2\pi/\Lambda_x = 3 \mu\text{m}$, $2\pi/\Lambda_y = 5 \mu\text{m}$, $H = 60 \mu\text{m}$, and $D_x = -40 \mu\text{m}$.

spectrum from the medium's resonant frequency. For the considered parameter set the instantaneous values of the angle θ defined as in Fig. 1 run over the range from $\pi/3$ at the nearest point of the layer down to approximately $0.493 \approx \pi/6.37$ at the most distant point. From the diagrams in Figs. 4 and 5 one can see that the divergence points for both Ω_1 and Ω_2 do not fall in this interval. Hence, the frequencies of the transient Cherenkov radiation fill the finite range with the boundaries determined from Eqs. (11) and (12) or diagrams in Figs. 4 and 5. Specifically, the frequency Ω_1 changes from $\Omega_1 = 2.51 \times 10^{15} \text{s}^{-1}$ as shown in Fig. 3 to $\Omega_1 = 1.08 \times 10^{15} \text{s}^{-1}$, while Ω_2 runs from $\Omega_2 = 5.63 \times 10^{15} \text{s}^{-1}$ in Fig. 3 to $\Omega_2 = 1.46 \times 10^{15} \text{s}^{-1}$. In total, the continuous range of the transient frequencies starting near $5.63 \times 10^{15} \text{s}^{-1}$ and extending up to 10^{15}s^{-1} is expected. The field spectrum in Fig. 10 confirms our calculations and yields the continuous frequency range with the predicted boundaries. This range also appears to be

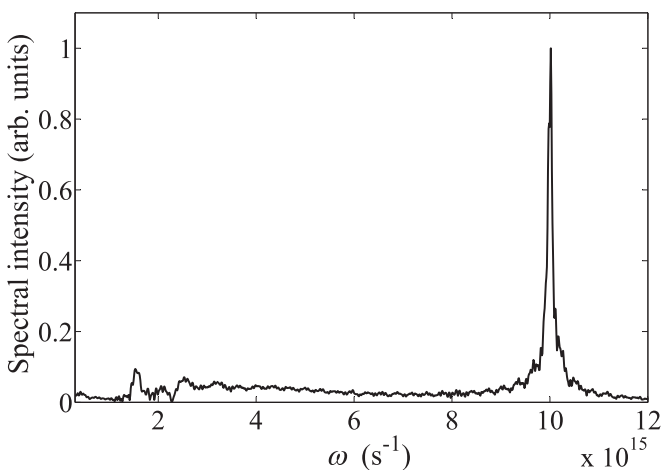


FIG. 10. Spectrum of the radiation from Fig. 9 for $\omega_0 = 10^{16} \text{s}^{-1}$.

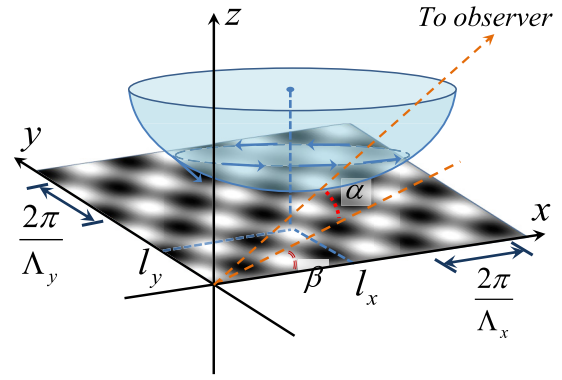


FIG. 11. An optically thin layer of a resonant medium with the spatially inhomogeneous density (the spatial frequencies of the density distribution are Λ_x and Λ_y over the x and y axes, respectively) is irradiated by an azimuthally polarized ultrashort pulse with the spherical wavefront (shaded blue). The source of the spherical wave is located at the point with coordinates l_x , l_y , and H . The medium radiation is detected at a distant point and the observation direction is determined by the angles α and β . The blue arrows show the direction of the electric-field vector in a certain cross section of the spherical wavefront.

significantly inhomogeneous and exhibits certain strong maxima which seem to originate from a varying part of the layer covered by the excitation pulse for each instantaneous value of the angle θ . One can see that the boundaries of the frequency range can be efficiently tuned by changing the location of the source of the cylindrical wave or the observation point. In such way we get huge flexibility in tuning the detected frequencies of Cherenkov radiation even without the necessity of changing the medium layer itself.

Next we proceed with the excitation by a spherical wave. For definiteness, the source of the spherical wave is assumed to be located at the height H above the plane of the array with the (x, y) coordinates l_x and l_y (see Fig. 11). Thus the delay function $\tau(x, y)$ attains the form

$$\tau(x, y) = \frac{R_0}{c} + \frac{\sqrt{H^2 + (x - l_x)^2 + (y - l_y)^2}}{c} - \cos \alpha \frac{x \cos \beta + y \sin \beta}{c}. \quad (17)$$

Equation (5) with the delay function (17) cannot be calculated analytically. However, based on the above results for a plane excitation wavefront, we can qualitatively determine certain expected spectral features of the measured radiation. In such an excitation geometry the excitation velocity is also varying with time, so instead of isolated additional frequencies (11) and (12) we get a whole range of frequencies filling an interval in the spectrum. Some features of this interval can be calculated directly using Eqs. (11) and (12). For instance, the largest value of the instantaneous excitation velocity is reached at a point located right below the source of the spherical wave, where the angle $\theta = \pi/2$, so the corresponding

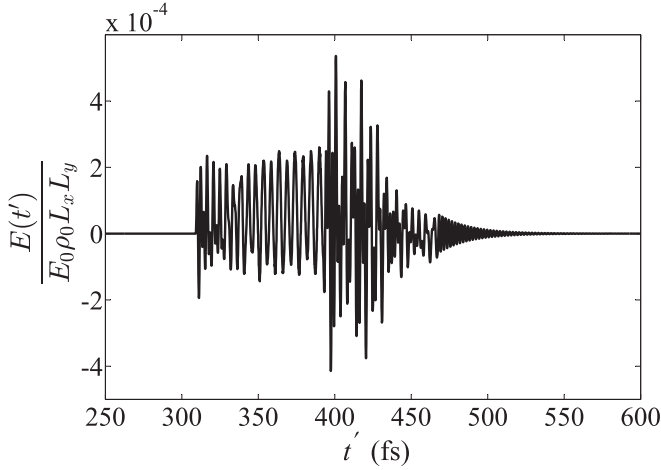


FIG. 12. Radiation from a thin layer of a spatially inhomogeneous medium shown in Fig. 11 for the parameter values $L_x = 60 \mu\text{m}$, $L_y = 50 \mu\text{m}$, $\omega_0 = 3 \times 10^{15} \text{ s}^{-1}$, $\gamma = 5 \times 10^{13} \text{ s}^{-1}$, $\alpha = 5\pi/12$, $\beta = \pi/4$, $A_x = A_y = 1$, $2\pi/\Lambda_x = 3 \mu\text{m}$, $2\pi/\Lambda_y = 5 \mu\text{m}$, $H = 60 \mu\text{m}$, $l_x = -50 \mu\text{m}$, and $l_y = -50 \mu\text{m}$.

instantaneous transient frequencies are

$$\begin{aligned}\Omega_1 &= -\frac{\Lambda_x c}{\cos \alpha \cos \beta}, \\ \Omega_2 &= -\frac{\Lambda_y c}{\cos \alpha \sin \beta}.\end{aligned}\quad (18)$$

However, further application of Eqs. (11) and (12) for the calculation of the instantaneous values of the transient Cherenkov frequencies is constrained by the polarization issues. Indeed, Eqs. (11) and (12) were derived assuming the linear polarization of the exciting plane wavefront. In the case of more complex polarizations of the excitation wave Eqs. (11) and (12) cannot be directly applied anymore due to the spatially varying factor (9) arising under the integration sign in Eq. (5). Here we suppose that our spherical excitation wavefront is azimuthally polarized as schematically shown in Fig. 11. Therefore, the angular factor $D(x, y, \alpha, \beta)$ attains the form

$$D(x, y, \alpha, \beta) = \sin \left[\arccos \left(\cos \alpha \frac{\tilde{x} \sin \beta - \tilde{y} \cos \beta}{\sqrt{\tilde{x}^2 + \tilde{y}^2}} \right) \right], \quad (19)$$

where we have introduced for convenience

$$\begin{aligned}\tilde{x} &= x - l_x, \\ \tilde{y} &= y - l_y.\end{aligned}$$

The integral (5) for the emitted field with the delay function (17), the spatial density (7), and the angular factor (19) was calculated numerically for several exemplary parameter values. One of the examples is depicted in Figs. 12 and 13. Figure 12 shows the measured electric field from the medium layer with the same size parameters as in Figs. 2, 3, 9, and 10, but excited by a spherical wavefront instead. Also, we have increased the medium resonant frequency to $\omega_0 = 3 \times 10^{15} \text{ s}^{-1}$ in order to make it easier to distinguish the frequencies of the transient Cherenkov radiation. Since

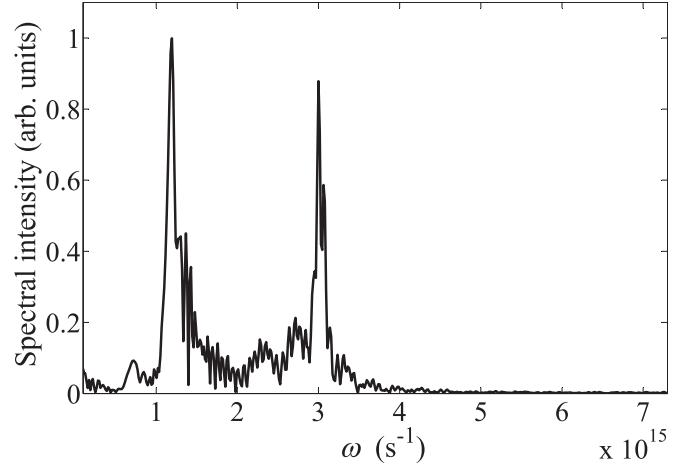


FIG. 13. Spectrum of the radiation from Fig. 12 for $\omega_0 = 3 \times 10^{15} \text{ s}^{-1}$.

the angle between the wavefront and the layer varies upon the pump pulse propagation over the medium, one can notice the complex nonregular character of the field oscillations in the transient stage. This fact is especially clearly seen in the frequency spectrum in Fig. 13. Here we get a wide continuous range of additional transient frequencies extending from almost the resonant frequency ω_0 up to the lower boundary around 10^{15} s^{-1} . Therefore, the transient Cherenkov radiation in the considered case possesses an ultrabroadband spectrum of more than one octave.

Finally, we move on to the case of a disk-shaped thin layer of a resonant medium with radially varying spatial density $\rho(r)$. In this case the integral (5) is reduced to the form

$$\begin{aligned}E(t) &= E_0 \int_0^R \int_0^{2\pi} e^{-\gamma(t-\tau(r,\phi))} \cos \omega_0(t - \tau(r, \phi)) \\ &\quad \times \Theta(t - \tau(r, \phi)) D(\vec{n}_E - \vec{n}_O) \rho(r) r dr d\phi,\end{aligned}\quad (20)$$

where (r, ϕ) are the polar coordinates, R is the radius of the disk, and the angular factor $D(\vec{n}_E - \vec{n}_O) = D(\varphi, \alpha, \beta)$ is given as

$$D(\phi, \alpha, \beta) = \sin\{\arccos[\cos \alpha \sin(\beta - \phi)]\}.\quad (21)$$

We suppose here that the disk-shaped layer of a resonant medium with the radius R is placed into the center of the coordinate system, while the source of the spherical excitation wave is located at the point with coordinates (l_x, l_y, H) . For the delay function $\tau(r, \phi)$ we get the expression

$$\begin{aligned}\tau(r, \phi) &= \frac{R_0}{c} + \sqrt{H^2 + (r \cos \phi - l_x)^2 + (r \sin \phi - l_y)^2} \\ &\quad \times \frac{1}{c} - \cos \alpha \cos(\phi - \beta) \frac{r}{c}.\end{aligned}\quad (22)$$

The spatial density of the medium's oscillators is taken to be radially varying and harmonic, similar to Eq. (7):

$$\rho(r) = \rho_0(1 + A_r \cos \Lambda_r r).\quad (23)$$

The integral (20) with the dependences (21)–(23) was numerically calculated for the parameters $R = 60 \mu\text{m}$, $A_r = 1$, $2\pi/\Lambda_r = 5 \mu\text{m}$, $H = 60 \mu\text{m}$, and different values of l_x and

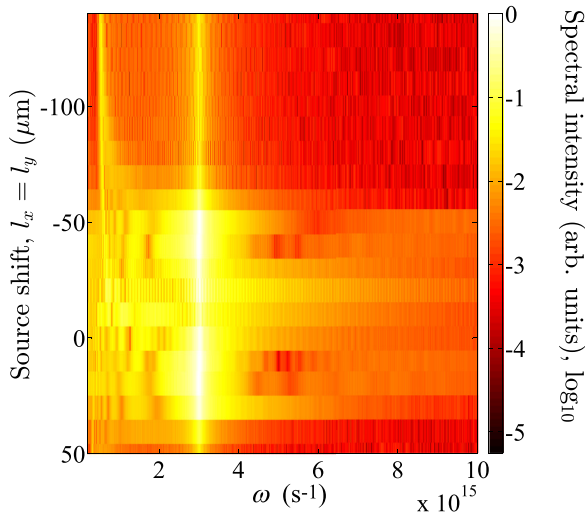


FIG. 14. Dependence of the radiation spectrum from a disk-shaped layer of a spatially inhomogeneous medium on the source shift $l_x = l_y$ for the parameter values $R = 60 \mu\text{m}$, $\omega_0 = 3 \times 10^{15} \text{ s}^{-1}$, $\gamma = 5 \times 10^{13} \text{ s}^{-1}$, $\alpha = 5\pi/12$, $\beta = \pi/4$, $A_r = 1$, $2\pi/\Lambda_r = 5 \mu\text{m}$, and $H = 60 \mu\text{m}$.

l_y . The results for a specific case of $l_x = l_y$ are shown in the diagram in Fig. 14, where the spectrum of the detected radiation is plotted vs the source shift $l_x = l_y$. One can see that an auxiliary spectral maximum of the transient Cherenkov radiation is especially pronounced, when a source is not located above the disk but is rather shifted aside. In Figs. 15 and 16 the obtained electric field and its spectrum are plotted for the parameter values $l_x = -100 \mu\text{m}$ and $l_y = -100 \mu\text{m}$. Besides a medium resonance we also get here a strong peak of the transient Cherenkov radiation near approximately $5.7 \times 10^{14} \text{ s}^{-1}$. As before, the strength and the central frequency of the Cherenkov peak can be varied by moving the source of the spherical wave and the observation direction, which allows efficient tuning of the transient Cherenkov radiation to a desired frequency.

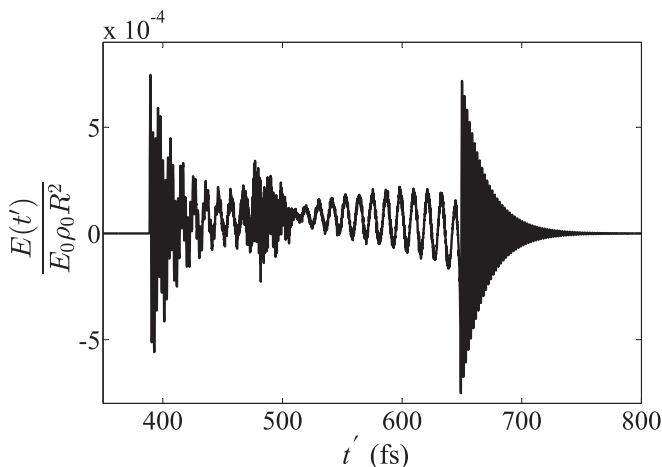


FIG. 15. Radiation from a disk-shaped layer of a spatially inhomogeneous medium for the parameter values $R = 60 \mu\text{m}$, $\omega_0 = 3 \times 10^{15} \text{ s}^{-1}$, $\gamma = 5 \times 10^{13} \text{ s}^{-1}$, $\alpha = 5\pi/12$, $\beta = \pi/4$, $A_r = 1$, $2\pi/\Lambda_r = 5 \mu\text{m}$, $H = 60 \mu\text{m}$, $l_x = -100 \mu\text{m}$, and $l_y = -100 \mu\text{m}$.

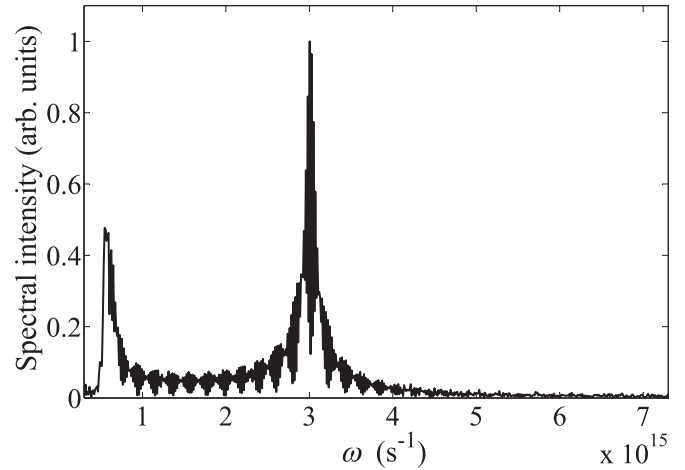


FIG. 16. Spectrum of the radiation from Fig. 15 for $\omega_0 = 3 \times 10^{15} \text{ s}^{-1}$.

V. CONCLUSION

We have investigated the transient Cherenkov radiation from a spatially inhomogeneous resonant medium being excited by an ultrashort pulse. This radiation is related to the collective phenomenon of the free-induction decay arising, when a thin layer of a medium is excited by an ultrashort pulse, which is shorter in duration than the medium coherence time T_2 . We have obtained that, by varying the medium geometry and/or the shape of the wavefront of the exciting wave, we can tune the frequency spectrum of the measured radiation in wide limits. Specifically, additional frequencies appear in a transient stage, i.e., while the excitation wavefront propagates over the medium layer. The inhomogeneity of the medium results in the varying number of oscillators contributing to the total optical response, which in turn leads to the signal modulation with the frequencies proportional to the spatial frequency of the medium's density variations.

Our findings provide a convenient approach for the frequency control of the Cherenkov radiation from a spatially inhomogeneous medium. While earlier studies yielded the possibility to tune the frequency of the Cherenkov radiation by changing the period of a photonic crystal, this was barely suitable to serve as a frequency-tunable or a swept-frequency source in applications since the period of a photonic crystal cannot be so rapidly and readily changed with time. In our setup the frequency of the detected Cherenkov radiation can be controlled not only by the period of the density distribution, but also through the excitation and observation geometry. Namely, by varying the shape of the excitation wavefront, the location of the excitation source and/or the observation direction, we can easily perform the control of the spectrum of the Cherenkov radiation. We expect therefore that the proposed scheme can be exploited to create an efficient and flexible compact source of frequency-tunable coherent radiation.

ACKNOWLEDGMENT

We acknowledge Russian Science Foundation for support through Project No. 17-19-01097.

APPENDIX

Here we present the calculation of the integral (5) with the periodic spatial density (7) and the delay function (8). Let us assume for definiteness that $q_x, q_y > 0$ and take for simplicity $\gamma = 0 \text{ s}^{-1}$. At the time period $t' < 0$, no field at the

observation point is detected, since the medium response has not yet reached the observer. Within the time interval $0 \leq t' < \min(q_x L_x, q_y L_y)$, the excitation wavefront propagates over the inhomogeneous array and starts the medium oscillators. In this case the exact calculation of the integral (5) yields

$$\begin{aligned} \frac{E(t)}{E_0 D \rho_0} &= \frac{q_x^2(1+A_x) - \Lambda_x^2}{q_x q_y (q_x^2 - \Lambda_x^2)} (1 - \cos \omega_0 t') + A_y q_y \frac{q_x^2(1+A_x) - \Lambda_x^2}{q_x (q_x^2 - \Lambda_x^2) (q_y^2 - \Lambda_y^2)} \left(\cos \frac{\Lambda_y \omega_0 t'}{q_y} - \cos \omega_0 t' \right) \\ &\quad - \frac{q_x A_x}{q_y (q_x^2 - \Lambda_x^2)} \left(1 - \cos \frac{\Lambda_x \omega_0 t'}{q_x} \right) - \frac{q_x q_y A_x A_y \Lambda_x^2}{(q_x^2 - \Lambda_x^2) (\Lambda_x^2 q_y^2 - \Lambda_y^2 q_x^2)} \left(\cos \frac{\Lambda_y \omega_0 t'}{q_y} - \cos \frac{\Lambda_x \omega_0 t'}{q_x} \right) \\ &= \frac{1}{q_x q_y} - \frac{[q_x^2(1+A_x) - \Lambda_x^2][q_y^2(1+A_y) - \Lambda_y^2]}{q_x q_y (q_x^2 - \Lambda_x^2) (q_y^2 - \Lambda_y^2)} \cos \omega_0 t' + \frac{q_x A_x [q_y^2 \Lambda_x^2 (1+A_y) - q_x^2 \Lambda_y^2]}{q_y (q_x^2 - \Lambda_x^2) (q_y^2 \Lambda_x^2 - q_x^2 \Lambda_y^2)} \cos \frac{\Lambda_x \omega_0 t'}{q_x} \\ &\quad + \frac{q_y A_y [q_x^2 \Lambda_y^2 (1+A_x) - q_y^2 \Lambda_x^2]}{q_x (q_y^2 - \Lambda_y^2) (q_x^2 \Lambda_y^2 - q_y^2 \Lambda_x^2)} \cos \frac{\Lambda_y \omega_0 t'}{q_y}, \end{aligned} \quad (\text{A1})$$

i.e., we get the terms oscillating at frequencies ω_0 , Ω_1 , and Ω_2 .

In the next stage, when $\min(q_x L_x, q_y L_y) \leq t' < \max(q_x L_x, q_y L_y)$, the excitation passes the array along one of the coordinate axes while still exciting along another axis. Therefore, instead of two additional frequencies of

the transient radiation (11) and (12) one obtains only one, which corresponds to the coordinate axis where the excitation wavefront has not yet reached the end of the array. If, for definiteness, we have $q_x L_x > q_y L_y$, then in the time interval $q_y L_y \leq t' < q_x L_x$ the integral (5) gives the terms oscillating at frequencies ω_0 and Ω_1 as follows:

$$\begin{aligned} E(t)/E_0 D \rho_0 &= \cos \omega_0 t' \frac{q_x^2(1+A_x) - \Lambda_x^2}{q_x q_y (q_x^2 - \Lambda_x^2)} \left(\cos q_y L_y - 1 + \frac{A_y q_y}{2(q_y - \Lambda_y)} [\cos(q_y - \Lambda_y)L_y - 1] \right. \\ &\quad \left. + \frac{A_y q_y}{2(q_y + \Lambda_y)} [\cos(q_y + \Lambda_y)L_y - 1] \right) + \sin \omega_0 t' \frac{q_x^2(1+A_x) - \Lambda_x^2}{q_x q_y (q_x^2 - \Lambda_x^2)} \left(\sin q_y L_y \right. \\ &\quad \left. + \frac{A_y q_y}{2(q_y - \Lambda_y)} \sin(q_y - \Lambda_y)L_y + \frac{A_y q_y}{2(q_y + \Lambda_y)} \sin(q_y + \Lambda_y)L_y \right) \\ &\quad + \cos \frac{\Lambda_x \omega_0 t'}{q_x} \frac{q_x A_x}{q_y (\Lambda_x^2 - q_x^2)} \left[\cos \frac{\Lambda_x q_y L_y}{q_x} - 1 + \frac{A_y \Lambda_x q_y}{2(\Lambda_x q_y - \Lambda_y q_x)} \left(\cos \frac{\Lambda_x q_y - \Lambda_y q_x}{q_x} L_y - 1 \right) \right. \\ &\quad \left. + \frac{A_y \Lambda_x q_y}{2(\Lambda_x q_y + \Lambda_y q_x)} \left(\cos \frac{\Lambda_x q_y + \Lambda_y q_x}{q_x} L_y - 1 \right) \right] + \sin \frac{\Lambda_x \omega_0 t'}{q_x} \frac{q_x A_x}{q_y (\Lambda_x^2 - q_x^2)} \left(\sin \frac{\Lambda_x q_y L_y}{q_x} \right. \\ &\quad \left. + \frac{A_y \Lambda_x q_y}{2(\Lambda_x q_y - \Lambda_y q_x)} \sin \frac{\Lambda_x q_y - \Lambda_y q_x}{q_x} L_y + \frac{A_y \Lambda_x q_y}{2(\Lambda_x q_y + \Lambda_y q_x)} \sin \frac{\Lambda_x q_y + \Lambda_y q_x}{q_x} L_y \right). \end{aligned}$$

Then, for $\max(q_x L_x, q_y L_y) \leq t' < q_x L_x + q_y L_y$ we again get varying integration limits over both axes. As a result, the oscillations again occur at all three frequencies ω_0 , Ω_1 , and Ω_2 . Indeed, assuming as before $q_x L_x > q_y L_y$, in the time interval $q_x L_x \leq t' < q_x L_x + q_y L_y$ we get, for the integral (5),

$$\begin{aligned} \frac{E(t)}{E_0 D \rho_0} &= -\frac{1}{q_x q_y} + \cos \omega_0 t' \left(\frac{q_x^2(1+A_x) - \Lambda_x^2}{q_x q_y (q_x^2 - \Lambda_x^2)} (\cos q_y L_y - 1) + A_y \frac{q_x^2(1+A_x) - \Lambda_x^2}{2q_x (q_y - \Lambda_y) (q_x^2 - \Lambda_x^2)} \right. \\ &\quad \times [\cos(q_y - \Lambda_y)L_y - 1] + A_y \frac{q_x^2(1+A_x) - \Lambda_x^2}{2q_x (q_y + \Lambda_y) (q_x^2 - \Lambda_x^2)} [\cos(q_y + \Lambda_y)L_y - 1] + \frac{1}{q_x q_y} \cos q_x L_x \\ &\quad + \frac{A_y q_y}{q_x (q_y^2 - \Lambda_y^2)} \cos q_x L_x + \frac{A_x}{2q_y (q_x + \Lambda_x)} \cos(q_x + \Lambda_x)L_x + \frac{A_x A_y q_y}{2(q_x + \Lambda_x) (q_y^2 - \Lambda_y^2)} \cos(q_x + \Lambda_x)L_x \\ &\quad \left. + \frac{A_x}{2q_y (q_x - \Lambda_x)} \cos(q_x - \Lambda_x)L_x + \frac{A_x A_y q_y}{2(q_x - \Lambda_x) (q_y^2 - \Lambda_y^2)} \cos(q_x - \Lambda_x)L_x \right) \end{aligned}$$

$$\begin{aligned}
 & + \sin \omega_0 t' \left(\frac{q_x^2(1 + A_x) - \Lambda_x^2}{q_x q_y (q_x^2 - \Lambda_x^2)} \sin q_y L_y + A_y \frac{q_x^2(1 + A_x) - \Lambda_x^2}{2q_x (q_y - \Lambda_y)(q_x^2 - \Lambda_x^2)} \sin(q_y - \Lambda_y)L_y \right. \\
 & + A_y \frac{q_x^2(1 + A_x) - \Lambda_x^2}{2q_x (q_y + \Lambda_y)(q_x^2 - \Lambda_x^2)} \sin(q_y + \Lambda_y)L_y + \frac{1}{q_x q_y} \sin q_x L_x + \frac{A_y q_y}{q_x (q_y^2 - \Lambda_y^2)} \sin q_x L_x \\
 & + \frac{A_x}{2q_y (q_x + \Lambda_x)} \sin(q_x + \Lambda_x)L_x + \frac{A_x A_y q_y}{2(q_x + \Lambda_x)(q_y^2 - \Lambda_y^2)} \sin(q_x + \Lambda_x)L_x \\
 & \left. + \frac{A_x}{2q_y (q_x - \Lambda_x)} \sin(q_x - \Lambda_x)L_x + \frac{A_x A_y q_y}{2(q_x - \Lambda_x)(q_y^2 - \Lambda_y^2)} \sin(q_x - \Lambda_x)L_x \right) \\
 & + \cos \frac{\Lambda_x \omega_0 t'}{q_x} \left(- \frac{q_x A_x}{q_y (q_x^2 - \Lambda_x^2)} \cos \frac{\Lambda_x q_y L_y}{q_x} - \frac{A_x A_y q_x \Lambda_x}{2(\Lambda_x q_y - \Lambda_y q_x)(q_x^2 - \Lambda_x^2)} \cos \frac{(\Lambda_x q_y - \Lambda_y q_x)L_y}{q_x} \right. \\
 & - \frac{A_x A_y q_x \Lambda_x}{2(\Lambda_x q_y + \Lambda_y q_x)(q_x^2 - \Lambda_x^2)} \cos \frac{(\Lambda_x q_y + \Lambda_y q_x)L_y}{q_x} \left. \right) \\
 & + \sin \frac{\Lambda_x \omega_0 t'}{q_x} \left(- \frac{q_x A_x}{q_y (q_x^2 - \Lambda_x^2)} \sin \frac{\Lambda_x q_y L_y}{q_x} - \frac{A_x A_y q_x \Lambda_x}{2(\Lambda_x q_y - \Lambda_y q_x)(q_x^2 - \Lambda_x^2)} \sin \frac{(\Lambda_x q_y - \Lambda_y q_x)L_y}{q_x} \right. \\
 & - \frac{A_x A_y q_x \Lambda_x}{2(\Lambda_x q_y + \Lambda_y q_x)(q_x^2 - \Lambda_x^2)} \sin \frac{(\Lambda_x q_y + \Lambda_y q_x)L_y}{q_x} \left. \right) \\
 & + \cos \frac{\Lambda_y \omega_0 t'}{q_y} \left[\frac{A_x A_y q_x \Lambda_x}{2(\Lambda_x q_y - \Lambda_y q_x)(q_x^2 - \Lambda_x^2)} \cos \frac{(\Lambda_x q_y - \Lambda_y q_x)L_y}{q_y} + \frac{A_x A_y q_x \Lambda_x}{2(\Lambda_x q_y + \Lambda_y q_x)(q_x^2 - \Lambda_x^2)} \right. \\
 & \times \cos \frac{(\Lambda_x q_y + \Lambda_y q_x)L_y}{q_y} - \frac{A_y q_y}{q_x (q_y^2 - \Lambda_y^2)} \cos \frac{\Lambda_y q_x L_x}{q_y} - \frac{A_x A_y}{4(q_x + \Lambda_x)(q_y - \Lambda_y)} \cos \left(\Lambda_x + \Lambda_y \frac{q_x}{q_y} \right) L_x \\
 & - \frac{A_x A_y}{4(q_x + \Lambda_x)(q_y + \Lambda_y)} \cos \left(\Lambda_x - \Lambda_y \frac{q_x}{q_y} \right) L_x - \frac{A_x A_y}{4(q_x - \Lambda_x)(q_y - \Lambda_y)} \cos \left(\Lambda_x - \Lambda_y \frac{q_x}{q_y} \right) L_x \\
 & \left. - \frac{A_x A_y}{4(q_x - \Lambda_x)(q_y + \Lambda_y)} \cos \left(\Lambda_x + \Lambda_y \frac{q_x}{q_y} \right) L_x \right] \\
 & + \sin \frac{\Lambda_y \omega_0 t'}{q_y} \left[- \frac{A_x A_y q_x \Lambda_x}{2(\Lambda_x q_y - \Lambda_y q_x)(q_x^2 - \Lambda_x^2)} \sin \frac{(\Lambda_x q_y - \Lambda_y q_x)L_y}{q_y} - \frac{A_x A_y q_x \Lambda_x}{2(\Lambda_x q_y + \Lambda_y q_x)(q_x^2 - \Lambda_x^2)} \right. \\
 & \times \sin \frac{(\Lambda_x q_y + \Lambda_y q_x)L_y}{q_y} - \frac{A_y q_y}{q_x (q_y^2 - \Lambda_y^2)} \sin \frac{\Lambda_y q_x L_x}{q_y} - \frac{A_x A_y}{4(q_x + \Lambda_x)(q_y - \Lambda_y)} \sin \left(\Lambda_x + \Lambda_y \frac{q_x}{q_y} \right) L_x \\
 & + \frac{A_x A_y}{4(q_x + \Lambda_x)(q_y + \Lambda_y)} \sin \left(\Lambda_x - \Lambda_y \frac{q_x}{q_y} \right) L_x + \frac{A_x A_y}{4(q_x - \Lambda_x)(q_y - \Lambda_y)} \sin \left(\Lambda_x - \Lambda_y \frac{q_x}{q_y} \right) L_x \\
 & \left. - \frac{A_x A_y}{4(q_x - \Lambda_x)(q_y + \Lambda_y)} \sin \left(\Lambda_x + \Lambda_y \frac{q_x}{q_y} \right) L_x \right].
 \end{aligned}$$

Finally, when $q_x L_x + q_y L_y \leq t'$ in the integral (5) we get only oscillations at the medium resonant frequency ω_0 ; hence the radiation spectrum in this case contains only one frequency:

$$\begin{aligned}
 \frac{E(t)}{E_0 D \rho_0} & = \cos \omega_0 t' \left(\frac{q_x^2(1 + A_x) - \Lambda_x^2}{q_x q_y (q_x^2 - \Lambda_x^2)} (\cos q_y L_y - 1) + A_y \frac{q_x^2(1 + A_x) - \Lambda_x^2}{2q_x (q_y - \Lambda_y)(q_x^2 - \Lambda_x^2)} [\cos(q_y - \Lambda_y)L_y - 1] \right. \\
 & + A_y \frac{q_x^2(1 + A_x) - \Lambda_x^2}{2q_x (q_y + \Lambda_y)(q_x^2 - \Lambda_x^2)} [\cos(q_y + \Lambda_y)L_y - 1] - \frac{1}{q_x q_y} [\cos(q_x L_x + q_y L_y) - \cos q_x L_x] \\
 & - \frac{A_y}{2q_x (q_y - \Lambda_y)} \{ \cos[q_x L_x + (q_y - \Lambda_y)L_y] - \cos q_x L_x \} - \frac{A_y}{2q_x (q_y + \Lambda_y)} \{ \cos[q_x L_x + (q_y + \Lambda_y)L_y] \\
 & - \cos q_x L_x \} - \frac{A_x}{2q_y (q_x + \Lambda_x)} \{ \cos[(q_x + \Lambda_x)L_x + q_y L_y] - \cos(q_x + \Lambda_x)L_x \} - \frac{A_x A_y}{4(q_x + \Lambda_x)(q_y - \Lambda_y)} \\
 & \times \{ \cos[(q_x + \Lambda_x)L_x + (q_y - \Lambda_y)L_y] - \cos(q_x + \Lambda_x)L_x \} - \frac{A_x A_y}{4(q_x + \Lambda_x)(q_y + \Lambda_y)}
 \end{aligned}$$

$$\begin{aligned}
& \times \left\{ \cos[(q_x + \Lambda_x)L_x + (q_y + \Lambda_y)L_y] - \cos(q_x + \Lambda_x)L_x - \frac{A_x}{2q_y(q_x - \Lambda_x)} \{ \cos[(q_x - \Lambda_x)L_x + q_y L_y] \right. \\
& - \cos(q_x - \Lambda_x)L_x \} - \frac{A_x A_y}{4(q_x - \Lambda_x)(q_y - \Lambda_y)} \{ \cos[(q_x - \Lambda_x)L_x + (q_y - \Lambda_y)L_y] - \cos(q_x - \Lambda_x)L_x \} \\
& - \frac{A_x A_y}{4(q_x - \Lambda_x)(q_y + \Lambda_y)} \{ \cos[(q_x - \Lambda_x)L_x + (q_y + \Lambda_y)L_y] - \cos(q_x - \Lambda_x)L_x \} \left. \right) \\
& + \sin \omega_0 t' \left(\frac{q_x^2(1 + A_x) - \Lambda_x^2}{q_x q_y (q_x^2 - \Lambda_x^2)} \sin q_y L_y + A_y \frac{q_x^2(1 + A_x) - \Lambda_x^2}{2q_x (q_y - \Lambda_y)(q_x^2 - \Lambda_x^2)} \sin(q_y - \Lambda_y)L_y \right. \\
& + A_y \frac{q_x^2(1 + A_x) - \Lambda_x^2}{2q_x (q_y + \Lambda_y)(q_x^2 - \Lambda_x^2)} \sin(q_y + \Lambda_y)L_y - \frac{1}{q_x q_y} [\sin(q_x L_x + q_y L_y) - \sin q_x L_x] \\
& - \frac{A_y}{2q_x (q_y - \Lambda_y)} \{ \sin[q_x L_x + (q_y - \Lambda_y)L_y] - \sin q_x L_x \} - \frac{A_y}{2q_x (q_y + \Lambda_y)} \{ \sin[q_x L_x + (q_y + \Lambda_y)L_y] \\
& - \sin q_x L_x \} - \frac{A_x}{2q_y (q_x + \Lambda_x)} \{ \sin[(q_x + \Lambda_x)L_x + q_y L_y] - \sin(q_x + \Lambda_x)L_x \} - \frac{A_x A_y}{4(q_x + \Lambda_x)(q_y - \Lambda_y)} \\
& \times \{ \sin[(q_x + \Lambda_x)L_x + (q_y - \Lambda_y)L_y] - \sin(q_x + \Lambda_x)L_x \} - \frac{A_x A_y}{4(q_x + \Lambda_x)(q_y + \Lambda_y)} \\
& \times \{ \sin[(q_x + \Lambda_x)L_x + (q_y + \Lambda_y)L_y] - \sin(q_x + \Lambda_x)L_x \} - \frac{A_x}{2q_y (q_x - \Lambda_x)} \{ \sin[(q_x - \Lambda_x)L_x + q_y L_y] \\
& - \sin(q_x - \Lambda_x)L_x \} - \frac{A_x A_y}{4(q_x - \Lambda_x)(q_y - \Lambda_y)} \{ \sin[(q_x - \Lambda_x)L_x + (q_y - \Lambda_y)L_y] - \sin(q_x - \Lambda_x)L_x \} \\
& \left. - \frac{A_x A_y}{4(q_x - \Lambda_x)(q_y + \Lambda_y)} \{ \sin[(q_x - \Lambda_x)L_x + (q_y + \Lambda_y)L_y] - \sin(q_x - \Lambda_x)L_x \} \right).
\end{aligned}$$

It is worth addressing the role of the nonzero damping rate γ of the medium oscillators. In such a case all calculations above become much more cumbersome; however, some general conclusions can still be made. First of all, all oscillation terms above would turn into damped oscillations. Therefore, the width of all spectral peaks would be increased due to the damping effect. This fact mainly limits the broadening of the spectral peak at the medium's

resonant frequency ω_0 , since the respective oscillations continue until getting completely stopped by the damping. At the same time, the spectral broadening of the transient Cherenkov peaks Ω_1 and Ω_2 is also limited by the finiteness of the time interval $0 \leq t' < q_x L_x + q_y L_y$, where the oscillations at these frequencies arise. Hence, the total broadening of these spectral peaks is determined by the mutual action of both factors.

-
- [1] P. A. Čerenkov, *Phys. Rev.* **52**, 378 (1937).
[2] J. V. Jelley, *Cerenkov Radiation and Its Applications* (Pergamon, London, 1958).
[3] B. M. Bolotovskii, *Phys. Usp.* **52**, 1099 (2009).
[4] Y. A. Bashmakov, *Phys. Usp.* **58**, 467 (2015).
[5] T. Ekelöf, J. Séguinot, J. Tocqueville, and T. Ypsilantis, *Phys. Scr.* **23**, 718 (1981).
[6] A. Ruggiero, J. P. Holland, J. S. Lewis, and J. Grimm, *J. Nucl. Med.* **51**, 1123 (2010).
[7] J. Zhong, C. Qin, X. Yang, S. Zhu, X. Zhang, and J. Tian, *Int. J. Biomed. Imaging* **2011**, 641618 (2011).
[8] S. Das, D. L. Thorek, and J. Grimm, in *Emerging Applications of Molecular Imaging to Oncology*, edited by M. G. Pomper and P. B. Fisher, Advances in Cancer Research (Academic, New York, 2014), Vol. 124, pp. 213–234.
[9] E. Branger, S. Grape, S. J. Svärd, P. Jansson, and E. A. Sundén, *J. Instrum.* **12**, T06001 (2017).
[10] E. Ciarrocchi and N. Belcari, *EJNMMI Phys.* **4**, 14 (2017).
[11] S. Liu, P. Zhang, W. Liu, S. Gong, R. Zhong, Y. Zhang, and M. Hu, *Phys. Rev. Lett.* **109**, 153902 (2012).
[12] M. I. Bakunov, A. V. Maslov, and S. B. Bodrov, *Phys. Rev. B* **72**, 195336 (2005).
[13] N. Akhmediev and M. Karlsson, *Phys. Rev. A* **51**, 2602 (1995).
[14] D. V. Skryabin and A. V. Gorbach, *Rev. Mod. Phys.* **82**, 1287 (2010).
[15] B. M. Bolotovskii and V. L. Ginzburg, *Sov. Phys. Usp.* **15**, 184 (1972).
[16] B. M. Bolotovskii and A. V. Serov, *Phys. Usp.* **48**, 903 (2005).
[17] V. L. Ginzburg, *Theoretical Physics and Astrophysics* (Elsevier, Amsterdam, 2013).
[18] R. M. Arkhipov, A. V. Pakhomov, M. V. Arkhipov, I. Babushkin, Y. A. Tolmachev, and N. N. Rosanov, *Laser Phys.* **27**, 053001 (2017).
[19] S. J. Smith and E. M. Purcell, *Phys. Rev.* **92**, 1069 (1953).

- [20] K. J. Woods, J. E. Walsh, R. E. Stoner, H. G. Kirk, and R. C. Fernow, *Phys. Rev. Lett.* **74**, 3808 (1995).
- [21] C. Luo, M. Ibanescu, S. Johnson, and J. Joannopoulos, *Science* **299**, 368 (2003).
- [22] C. Kremers, D. N. Chigrin, and J. Kroha, *Phys. Rev. A* **79**, 013829 (2009).
- [23] V. V. Vorobev and A. V. Tyukhtin, *Phys. Rev. Lett.* **108**, 184801 (2012).
- [24] V. Ginis, J. Danckaert, I. Veretennicoff, and P. Tassin, *Phys. Rev. Lett.* **113**, 167402 (2014).
- [25] Z. Su, B. Xiong, Y. Xu, Z. Cai, J. Yin, R. Peng, and Y. Liu, *Adv. Opt. Mater.* **7**, 1801666 (2019).
- [26] T. E. Stevens, J. K. Wahlstrand, J. Kuhl, and R. Merlin, *Science* **291**, 627 (2001).
- [27] J.-K. So, J.-H. Won, M. Sattarov, S.-H. Bak, K.-H. Jang, G.-S. Park, D. Kim, and F. Garcia-Vidal, *Appl. Phys. Lett.* **97**, 151107 (2010).
- [28] D. E. Fernandes, S. I. Maslovski, and M. G. Silveirinha, *Phys. Rev. B* **85**, 155107 (2012).
- [29] T. A. Morgado, D. E. Fernandes, and M. G. Silveirinha, *Photonics* **2**, 702 (2015).
- [30] F. Liu, L. Xiao, Y. Ye, M. Wang, K. Cui, X. Feng, W. Zhang, and Y. Huang, *Nat. Photon.* **11**, 289 (2017).
- [31] H. Hu, X. Lin, J. Zhang, D. Liu, P. Genevet, B. Zhang, and Y. Luo, *Laser Photon. Rev.* **14**, 2000149 (2020).
- [32] S. Xi, H. Chen, T. Jiang, L. Ran, J. Huangfu, B.-I. Wu, J. A. Kong, and M. Chen, *Phys. Rev. Lett.* **103**, 194801 (2009).
- [33] Z. Duan, Z. Wang, Y. Zhang, X. Chen, M. Chen, and Y. Gong, *Nat. Commun.* **8**, 14901 (2017).
- [34] W. Li, J. Liu, Y. Gao, K. Zhou, and S. Liu, *Opt. Lett.* **45**, 315 (2020).
- [35] Y. Song, N. Jiang, L. Liu, X. Hu, and J. Zi, *Phys. Rev. Appl.* **10**, 064026 (2018).
- [36] T. Denis, M. W. van Dijk, J. H. H. Lee, R. van der Meer, A. Strooisma, P. J. M. van der Slot, W. L. Vos, and K.-J. Boller, *Phys. Rev. A* **94**, 053852 (2016).
- [37] R. M. Arkipov, I. Babushkin, M. K. Lebedev, Y. A. Tolmachev, and M. V. Arkipov, *Phys. Rev. A* **89**, 043811 (2014).
- [38] R. M. Arkipov, M. V. Arkipov, I. Babushkin, and Y. A. Tolmachev, *Quantum Electron.* **45**, 590 (2015).
- [39] R. Arkipov, M. Arkipov, P. Belov, I. Babushkin, and Y. A. Tolmachev, *Opt. Spectrosc.* **120**, 423 (2016).
- [40] R. Arkipov and A. Pakhomov, *Opt. Spectrosc.* **122**, 768 (2017).
- [41] L. Allen and J. H. Eberly, *Optical Resonance and Two-Level Atoms* (Wiley, New York, 1975).
- [42] M. Felici, P. Gallo, A. Mohan, B. Dwir, A. Rudra, and E. Kapon, *Small* **5**, 938 (2009).
- [43] A. Mohan, M. Felici, P. Gallo, B. Dwir, A. Rudra, J. Faist, and E. Kapon, *Nat. Photon.* **4**, 302 (2010).
- [44] G. Juska, V. Dimastrodonato, L. Mereni, A. Gocalinska, and E. Pelucchi, *Nat. Photon.* **7**, 527 (2013).
- [45] L. Novotny and N. Van Hulst, *Nat. Photon.* **5**, 83 (2011).
- [46] P. Biagioni, J.-S. Huang, and B. Hecht, *Rep. Prog. Phys.* **75**, 024402 (2012).
- [47] J. Sun, E. Timurdogan, A. Yaacobi, E. Hosseini, and M. Watts, *Nature (London)* **493**, 195 (2013).
- [48] R. M. Arkipov, A. V. Pakhomov, M. V. Arkipov, A. Demircan, U. Morgner, N. N. Rosanov, and I. Babushkin, *Phys. Rev. A* **101**, 043838 (2020).
- [49] R. Arkipov, M. Arkipov, I. Babushkin, A. Pakhomov, and N. Rosanov, *Opt. Spectrosc.* **128**, 1857 (2020).
- [50] R. Arkipov, M. Arkipov, A. Pakhomov, M. Zhukova, A. Tcypkin, and N. Rosanov, *JETP Lett.* **113**, 242 (2021).
- [51] A. V. Pakhomov, R. M. Arkipov, I. V. Babushkin, N. N. Rosanov, and M. V. Arkipov, *Laser Phys. Lett.* **13**, 126001 (2016).
- [52] A. V. Pakhomov, R. M. Arkipov, I. V. Babushkin, M. V. Arkipov, Y. A. Tolmachev, and N. N. Rosanov, *Phys. Rev. A* **95**, 013804 (2017).
- [53] L. D. Landau and E. M. Lifshitz, *The Classical Theory of Fields* (Butterworth-Heinemann, Oxford, 1980).